DTU Wind Energy E-Report-0221

GASP Uncertainty Classification

Xiaoli Guo Larsén, Marc Imberger, Neil Davis, Mark Kelly, Ásta Hannesdóttir

DTU Wind Energy
Department of Wind Energy

DTU Wind Energy, Risø Campus,
Technical University of Denmark, Roskilde, Denmark

June 2021

Author: Xiaoli Guo Larsén, Marc Imberger, Neil Davis, Mark Kelly, Ásta Hannesdóttir
Title: GASP Uncertainty Classification
Department: DTU Wind Energy

DTU Wind Energy E-Report-0221
June 23, 2021

ISSN:978-87-93549-89-0

Project no:
EUDP 64018-0095

Sponsorship:

Cover:-

Tables: 3
Figures: 11
References: 9

Technical University of Denmark
Frederiksborgvej 399
4000 Roskilde
Denmark
Tel. +4546775024
xgal@dtu.dk
www.vindenergi.dtu.dk

Contents

1 Introduction

This report describes a simple method for categorizing uncertainties of two key siting parameters, the 50-year wind and the turbulence intensity. The assessment closely follows the methodologies and data that are used for calculating the two siting parameters. The methodologies are described in Larsén et al. (2021). This is a simple method in a sense that uncertainty categories are estimated, rather than probabilities of targeted parameters. This is seen as a necessary and a efficient approach for the GASP project, as there are many sources of input data and the quality assessment is in general absent or only qualitatively available. In addition, the GASP calculations are done over the entire globe using one consistent methodology. This methodology, including many layers of sub-methods, is challenged to different degrees in different areas, due to different flow natures and complexities for modeling. At the same time, the available measurements are too few to guide us toward a typical uncertainty assessment global-wise. These, altogether, makes it difficult to quantify the overall effects from the many uncertainty contributors in terms of probabilities.

The methods for the uncertainty assessment are introduced in Sect. 2 and a presentation of the final uncertainty class layer is provided in Sect. 3.

2 Methods

2.1 Introduction of Uncertainty Index UI

As a consequence of the challenges addressed in Sect. 1, the uncertainty assessment will make use of a uncertainty classification strategy instead of a classical uncertainty quantification. We describe the uncertainty in three categories, borrowing the traffic light principles, with green as reliable, orange with higher uncertainty and red not reliable based on the definition of a uncertainty index UI:

$$UI = \frac{\sum_{i=1}^{N} c_i \cdot UI_i}{\sum_{i=1}^{N} c_i} \tag{1}$$

Depending on the impact of each contributor i on the calculation of the 50-year wind and the turbulence to a given grid point, we assign an uncertainty index UI_i ranging from 1 to 3, and a corresponding weighting coefficient c_i. Thus, the overall uncertainty index is obtained by summing over the total number of contributors. An uncertainty index 1 means low uncertainty, 2 means medium and 3 means high uncertainty. Each step of our calculation toward the final results contributes to uncertainty. Please refer to Larsén et al. (2021) for relevant algorithms involved in the calculations. Following these algorithms, there are specific contributors to the calculation of the 50-year winds as well as to the two methods for turbulence, see Sections 2.3 and 2.4, respectively.

The determination of such an "impact" and thereof the assignment of UI_i and c_i are rather empirical here. Due to the extremely heavy calculation over the whole globe, it is not possible to test how each input parameter and their combinations contribute to a distribution of the final estimation of either the 50-year wind or the turbulence. Rather, the determination is built on a small sample of sensitivity tests and documented quality measure for different data and different methods. However, these assigned numbers can be adjusted easily once there are studies to update them. A detailed overview of the assigned uncertainty indices and weights is dependent on the siting parameter and are presented in Sect. 2.3 (50-year wind) and Sect. 2.4 (turbulence), respectively.

2.2 Definition of Area Classes

The uncertainties related to the data and methods are different in different regions or areas with certain characteristics (land, water, terrain complexity, etc.). Thus, as a first step, we define a number of areas, summarized in Table 1. In this table, 16 characteristic areas are defined based on the land-sea surface, the terrain complexity, the effect from the roughness length speedup and the distance from the coastline over water or over land. The first three factors are related to the use of the Linear Computational Model (LINCOM) and the last one is related to the coastal smoothing approach that is used to merge two different methods applied to land and water areas, respectively. In principal, it would be possible to add more characteristic areas to the list, or remove from it, if, for instance, corresponding data or methods are changed, causing the uncertainty level to change.

The performance of LINCOM is in general reliable for simple land terrain, acceptable for moderately complex terrain (reliably overpredicting speedups), and unreliable for complex terrain. The terrain complexity here is defined firstly by the so-called "Ruggedness Index" (*RIX*). Expressed as a percentage or decimal, it is determined as the fraction of terrain exceeding a slope of 30% (about 17°), calculated as an areal average (omnidirectionally) within a circle of radius of 3.5 km (Mortensen et al., 2006) around a given point. Table 2 shows that we have used *RIX* values of 0.03 and 0.10 to separate terrain into three categories: simple, medium-complex and complex.

The second index for terrain complexity used here is the speedup caused by roughness length change. This is also related to the reliability of the LINCOM function, where higher uncertainty is expected where unusual high speedup effect related to sharp change in roughness length over the space are present. Two categories are defined accordingly using a critical threshold of 2% (see Table 2) to separate areas with low roughness speedup ($\leq 2\%$) and high roughness speedup ($>2\%$).

Over water, the LINCOM model is not applied; the generalization procedure is not applied and the roughness length is derived as a function of wind speed, where the high wind speed effect is considered. Over coastal land areas, the generalization and the use of LINCOM result in unrealistic estimations of the wind (see Table 2). A two-step process has been used to replace unrealistic estimations over land: Firstly, the offshore data based on the CFSR data set has been extended further inland using the so called "Creep filling" extrapolation technique from the Earth System Modeling Framework[1] (ESMF, Hill et al., 2004, Version 8.0.1). Subsequently, LINCOM winds within 50 km from the coastline are replaced by the creep-filled offshore winds if the following conditions are met: (1) LINCOM winds are stronger than offshore winds and (2) the site-elevation is below 500 m. While this correction has only been applied to the 50-year winds, the reduced reliability of LINCOM over coastal land areas and and the creep filling method has been the main driver for the distinction of coastal land/water and far inland/offshore regions.

Combining the definitions provided in Table 1 and Table 2, each data point can be attributed to a certain area ID. Figure 2 shows the histogram of area IDs for the three heights 50 m, 100 m and 150 m and a spatial depiction of the area IDs at 50-m height for an example region (UTM zone 32V). Due to the height dependence of the maximum roughness speedup, the shares of area IDs associated with land (category 1 to 12) vary with height as well. This means that a particular latitude/longitude over land might see different area IDs at different heights. The allocation of area IDs is the same for the assessment 50-year wind and the turbulence models.

[1] `https://www.earthsystemcog.org/projects/esmf/`

Table 1: Area ID and corresponding characteristics

ID	Land/Sea	Terrain	Roughness Speedup	Coastal
1	land	simple	low roughness speedup	
2	land	medium complex	low roughness speedup	
3	land	complex	low roughness speedup	
4	land	simple	high roughness speedup	
5	land	medium complex	high roughness speedup	
6	land	complex	high roughness speedup	
7	land	simple	low roughness speedup	coastal
8	land	medium complex	low roughness speedup	coastal
9	land	complex	low roughness speedup	coastal
10	land	simple	high roughness speedup	coastal
11	land	medium complex	high roughness speedup	coastal
12	land	complex	high roughness speedup	coastal
13	water	open water		
14	water			simple coastal
15	water	tropical cyclone affected area		
16	water			complex coastal

Table 2: Definitions of terms used in Table 1

Term	Definition
Simple terrain	$RIX \leq 0.03$
Medium complex terrain	$0.03 < RIX \leq 0.10$
Complex terrain	$RIX > 0.10$
Low roughness speedup	maximum roughness speedup (over all sectors) ≤ 0.02
High roughness speedup	maximum roughness speedup (over all sectors) > 0.02
Coastal land	land area that is ≤ 50 km away from the nearest coastline
Coastal water, simple	water point that is ≤ 50 km away from the nearest coastline and $RIX \leq 0.05$
Coastal water, complex	water point that is ≤ 50 km away from the nearest coastline and $RIX > 0.05$
Open water	water point that is > 50 km away from the nearest coastline

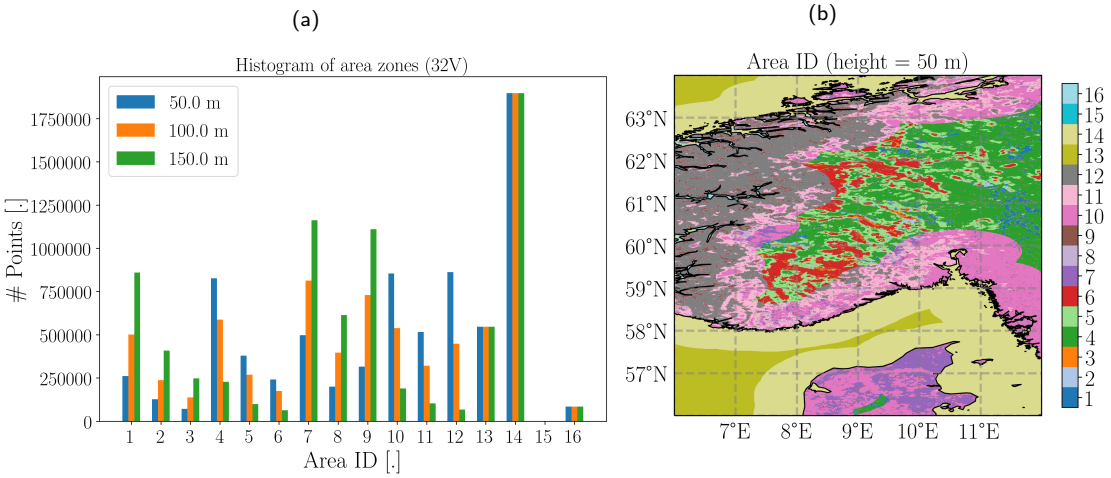

Figure 2: Distribution of area IDs within UTM zone 32V (cf. Fig. 1 in Larsén et al. (2021)): (a) Histogram for the three heights 50 m, 100 m and 150 m and (b) spatial distribution. The definition of area IDs follows Table 1.

2.3 The uncertainty classification of the calculation of the 50-year wind

Toward the final results of the 50-year wind at 50 m, 100 m and 150 m, at a spatial resolution of 250 m and an effective temporal resolution of 10 min, the main functions include:

- Generalization
- Spectral correction
- Creep filling and combining
- LINCOM downscaling
- Gumbel distribution

And the data include:

- Climate Forecast System Reanalysis (CFSR, (Saha et al., 2010)) covering 1979–2010
- SRTM 3 arc-sec/Viewfinder
- ESA CCI Land cover (ESA CCI-LC[2], ESA (2017))

As introduced in Larsén et al. (2021), we compared four reanalysis products (CFSR, ERA5, CFDDA and MERRA) for two regions, Europe and South Africa, and found that CFSR performs best in comparison with measurements. It is however not assessed how much uncertainty each reanalysis product provides and it is certainty not possible for us to do it on a global scale due to lack of measurements. We therefore assume CFSR quality is the same over the whole globe and will leave it out of the algorithms for calculating the final UI.

All functions and remaining data are used as contributors to the uncertainty, and they are listed in Fig. 3 as

1. *RIX* number
2. Terrain quality: The simpler terrain, the less uncertainty it can bring to the whole calculation
3. Roughness quality: The simpler terrain, the higher reliability of the roughness length data.
4. LINCOM. Note that LINCOM is not applied over water areas.
5. Creep filling and combining: The creep-filling extrapolation method itself affects the coastal water, while the replacing and combining procedure (as described in 2.2) affects the coastal land area. Note that this method does not affect inland areas or open seas far away from the coastline.
6. Spectral correction.
7. Generalization. Note that this is not applied to water areas.
8. Gumbel fit: uncertainty related to the 95% confidence level of the Gumbel fit.

A suit of values of uncertainty indices from the above contributors are assigned to all grid points that are grouped into the 16 area IDs (Fig. 3). Indices between 1 and 3 are assigned to grid points that satisfy conditions of the orange boxes. The white boxes indicate that there are no contributions from those groups of grid points with that area ID (e.g. no contribution of LINCOM to water points).

For the gray boxes, here only the contributor "Gumbel fit", the uncertainty index depends on the relative ratio $r = \sigma_{U_{50}}/U_{50}$ for the grid point and needs to be calculated therefore dynamically for each point individually. Figure 4 shows the global distribution of the ratio r. For the dynamic calculation, we assign $UI_i = 1$ for $r < 0.04$, $UI_i = 1.5$ for $0.04 \leq r < 0.07$, $UI_i = 2$ for $0.07 \leq r < 0.1$, $UI_i = 2.5$ for $0.1 \leq r < 0.2$ and $UI_i = 3$ for $r \geq 0.2$.

[2]http://maps.elie.ucl.ac.be/CCI/viewer/download.php

Uncertainty Index Matrix (data quality, contains values between 1 (green category,low uncertainty) and 3 (red, high uncertainty))								
	Uncertainty for certain area category associated with...							
Area ID	RIX number	Terrain quality	roughness quality	LINCOM	Creep filling + combining	Spectral Correction	Generalizatio n	Gumbel fit
1	1.0	1.0	1.5	1.0	nan	1.0	1.0	nan
2	1.5	1.5	1.5	1.5	nan	1.5	1.5	nan
3	3.0	3.0	1.5	2.5	nan	3.0	3.0	nan
4	1.0	1.0	2.5	1.0	nan	1.0	1.0	nan
5	2.0	2.0	2.5	1.5	nan	1.5	2.0	nan
6	3.0	3.0	2.5	2.5	nan	3.0	3.0	nan
7	1.0	1.0	1.5	3.0	1.5	1.0	2.0	nan
8	1.5	2.0	1.5	3.0	1.5	1.5	1.5	nan
9	3.0	3.0	1.5	3.0	2.0	2.5	3.0	nan
10	1.0	1.0	2.5	3.0	1.5	1.0	2.0	nan
11	2.0	2.0	2.5	3.0	1.5	2.0	2.0	nan
12	3.0	3.0	2.5	3.0	2.0	3.0	3.0	nan
13	1.0	1.0	1.0	nan	nan	1.0	nan	nan
14	1.0	3.0	1.5	nan	3.0	1.5	nan	nan
15	1.0	2.0	2.5	nan	nan	2.5	nan	nan
16	1.5	3.0	2.5	nan	3.0	3.0	nan	nan

Figure 3: Uncertainty index matrix for the 50-year wind with contributions of eight parameters. Orange: Modifiable static values. Gray: Dynamically allocated. White: no values.

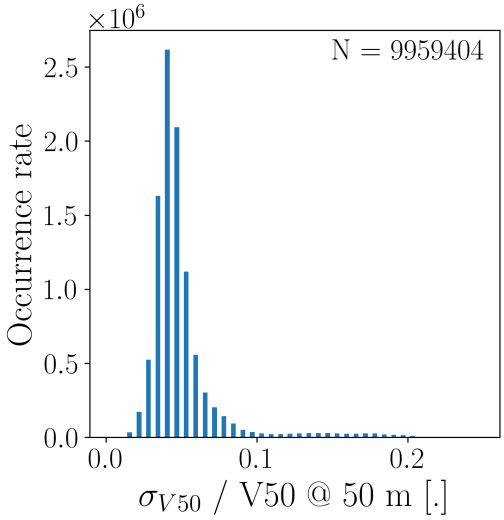

Figure 4: Distribution of the ratio $\sigma_{U_{50}}/U_{50}$ at 50 m based on a sampled sub-set from the global data set (every 20-th point in south-north and west-east direction within the definition range of the GASP data set). The total sample size N used for the histogram is stated in the top-right.

For each of the UI_i assigned in Fig. 3, a weighting coefficient c_i is assigned accordingly in Fig. 5 with the purpose to classify the share of different contributors on certain areas.

Thus, for the 50-year wind at a spatial resolution of 250 m and a temporal resolution of 10 min, the overall uncertainty index UI can be calculated with Eq. 1 where $N = 8$.

Matrix of Weights (contains values between 0 (no impact) and 1 (fully dominating))								
	Weight associated with a certain uncertainty category ...							
Area ID	RIX number	Terrain quality	roughness quality	LINCOM	Creep filling + combining	Spectral Correction	Generalizatio n	Gumbel fit
1	0.29	0.04	0.11	0.25	0.00	0.11	0.14	0.07
2	0.29	0.04	0.11	0.25	0.00	0.11	0.14	0.07
3	0.29	0.04	0.11	0.25	0.00	0.11	0.14	0.07
4	0.29	0.04	0.11	0.25	0.00	0.11	0.14	0.07
5	0.29	0.04	0.11	0.25	0.00	0.11	0.14	0.07
6	0.29	0.04	0.11	0.25	0.00	0.11	0.14	0.07
7	0.28	0.03	0.10	0.24	0.03	0.10	0.14	0.07
8	0.28	0.03	0.10	0.24	0.03	0.10	0.14	0.07
9	0.28	0.03	0.10	0.24	0.03	0.10	0.14	0.07
10	0.28	0.03	0.10	0.24	0.03	0.10	0.14	0.07
11	0.28	0.03	0.10	0.24	0.03	0.10	0.14	0.07
12	0.28	0.03	0.10	0.24	0.03	0.10	0.14	0.07
13	0.39	0.17	0.17	0.00	0.00	0.17	0.00	0.11
14	0.29	0.13	0.13	0.00	0.25	0.13	0.00	0.08
15	0.39	0.17	0.17	0.00	0.00	0.17	0.00	0.11
16	0.29	0.13	0.13	0.00	0.25	0.13	0.00	0.08

Figure 5: Weighting coefficients corresponding to the eight parameters for the calculation of the 50-year wind. Legends are the same as Fig. 3

2.4 The uncertainty of the calculation of turbulence

The turbulence parameters that are used in connection with load calculations are: (1) the coefficients a and b in the linear relation $TI = a \cdot U + b$, where TI is the turbulence intensity; (2) the coefficients a_σ and b_σ in the analogous linear relation for variability of turbulence 'strength' $\sigma_{\sigma_U} = a_\sigma \cdot U + b_\sigma$.

We used two methods to calculate the turbulence parameters in GASP. The corresponding uncertainty classification methods are shown below in Sections 2.4.1 and 2.4.2, respectively.

2.4.1 Method-1

Toward the final estimations of the two pairs of coefficients (a, b) and (a_σ, b_σ) in method 1, the main functions include:

- The use of the Kaimal spectral turbulence model for the along-wind component for all three heights.
- We used a low frequency limit at $f = 1$ h^{-1} for the integration of the Kaimal model when calculating σ_u.
- Wavelet filtering to smooth values cross data tiles.
- The linear regressions are done over two wind speed ranges [5, 30] m s^{-1} and [10, 40] m s^{-1}, respectively, forming two calculations.
- σ_{σ_U} is obtained by generating a population/spread of σ_U using the directional data population.
- We ignored the effect of stability.

The main data include:

- Data sets from Global Wind Atlas 3 (GWA3, https://globalwindatlas.info/): sectorwise distribution of mean wind speed and occurrence frequencies, z_{0meso}, all at a spatial resolution of 250 m.
- Roughness length over land grid point: z_{0meso}
- Roughness length over water grid point: derived from the algorithm used in the wave model SWAN (cf. methodology in Larsén et al. (2021)), where the drag coefficient C_D is a function of wind speed: it decreases with wind speed first in the smooth flow regime, increases with wind speed up to about 32 m s^{-1}, levels off and started decreasing for stronger wind speed.

In the following, six contributors to the corresponding uncertainty are thus defined and they are listed in Fig. 6:

- Roughness length in connection with the use of the Kaimal model.
- The low cut-off frequency for integrating the spectrum. It would make better sense if we could make it a function of height, instead of using one constant $f = 1$ h^{-1} for conditions, as this quantity is related to the size of boundary-layer eddies and the height of the boundary layer. However, the current database lacks important information such as stability for us to assess these scales. The use of $f = 1$ h^{-1} is more uncertain for higher elevations where it can be even questionable if the Kaimal turbulence model is valid any longer. UI_i from this contributor is height dependent (and therfore dynamically updated) and chosen to be 1.5 for 50 m, 2.0 for 100 m and 2.5 for 150 m.
- Directional distribution of the mean wind speed.
- Linear coefficients: It is known that in the smooth-flow regime, TI decreases with increasing wind speed. Convection occurs sometimes at relatively weak winds, corresponding to instability and strong turbulence. These characteristics can not be captured by the simple one-order linear regression. Thus we assign higher uncertainty index to light winds less than 5 m s^{-1} (dynamic allocation).
- Stability
- Wavelet filtering.

Uncertainty Index Matrix (contains values between 1 (green category,low uncertainty) and 3 (red, high uncertainty))						
	Uncertainty for certain area category associated with…					
Area ID	Kaimal model (z0) land water	Kaimal model cut off frequency	Mean wind sector-wise distribution GWA	Linear coefficients	Stability	Wavelet Filtering
1	1.5	nan	1.0	nan	2.0	2.0
2	2.0	nan	2.0	nan	2.0	2.0
3	3.0	nan	3.0	nan	2.0	2.0
4	1.5	nan	1.0	nan	2.0	2.0
5	2.0	nan	2.0	nan	2.0	2.0
6	3.0	nan	3.0	nan	2.0	2.0
7	1.5	nan	1.0	nan	2.0	2.0
8	2.0	nan	2.0	nan	2.0	2.0
9	3.0	nan	3.0	nan	2.0	2.0
10	1.5	nan	1.0	nan	2.0	2.0
11	2.0	nan	2.0	nan	2.0	2.0
12	3.0	nan	3.0	nan	2.0	2.0
13	1.0	nan	1.0	nan	2.0	2.0
14	1.0	nan	1.0	nan	2.0	2.0
15	2.0	nan	2.0	nan	2.0	2.0
16	2.0	nan	2.0	nan	2.0	2.0

Figure 6: Uncertainty index matrix for turbulence (method-1) with contributions of six parameters. Legends are the same as Fig. 3

The corresponding UI_i from these contributors are assigned to the 16 area categories, as shown in Fig. 6. The algorithms behind the values for the gray boxes are explained in the list above. The corresponding weighting coefficients are assigned in Fig. 7. One can see that we assigned UI_i of 2 from the stability effect for all 16 categories, but assigned 0% weight to it. This is because we did not include stability effect in the calculation due to missing input information. This contribution is however included in the algorithms for uncertainty assessment, in case in the future, or for some areas, there is input information available. Similar conditions motivated the omission of

Matrix of Weights (contains values between 0 (no impact) and 1 (fully dominating))						
	Weight associated with a certain uncertainty category …					
Area ID	Kaimal model (z0) land water	Kaimal model cut off frequency	Mean wind sector-wise distribution GWA	Linear coefficients	Stability	Wavelet Filtering
1	0.40	0.10	0.30	0.20	0.00	0.00
2	0.40	0.10	0.30	0.20	0.00	0.00
3	0.40	0.10	0.30	0.20	0.00	0.00
4	0.40	0.10	0.30	0.20	0.00	0.00
5	0.40	0.10	0.30	0.20	0.00	0.00
6	0.40	0.10	0.30	0.20	0.00	0.00
7	0.40	0.10	0.30	0.20	0.00	0.00
8	0.40	0.10	0.30	0.20	0.00	0.00
9	0.40	0.10	0.30	0.20	0.00	0.00
10	0.40	0.10	0.30	0.20	0.00	0.00
11	0.40	0.10	0.30	0.20	0.00	0.00
12	0.40	0.10	0.30	0.20	0.00	0.00
13	0.40	0.10	0.30	0.20	0.00	0.00
14	0.40	0.10	0.30	0.20	0.00	0.00
15	0.40	0.10	0.30	0.20	0.00	0.00
16	0.40	0.10	0.30	0.20	0.00	0.00

Figure 7: Weighting coefficients corresponding to the six parameters in Fig. 6. Legends are the same as Fig. 3

the wavelet filter impacts, where the uncertainty on spatial extend and impact strength would result in unjustifiable jumps of uncertainty classes at tile borders when UIs are close to the class thresholds. This exaggeration of the impact of the filtering at the tile border is not intended and after more detailed assessment on the global data set, it has therefore been decided to keep the wavelet filtering as a contributor but to omit its contribution (i.e. weight 0%) at the current stage.

The overall UI can thus be calculated with Eq. 1 with $N = 6$.

2.4.2 Method-2

Again using the 16 different categories of surface/flow-regime shown in Table 1, we calculate the uncertainty class by multiplying the category matrix by a matrix of weights for the turbulence calculation method driven by shear and terrain complexity (Kelly, 2020). However, in this case the 'weights' are dynamic, obtained from normalized (dimensionless) sensitivities following from the ISO-standard Guide for Uncertainty in Measurements (JCGM, 2008) and wind energy application as in Kelly et al. (2019). That means uncertainty estimates which follow from Uncertainty Quantification (UQ) of the turbulence model components and inputs (considering their aleatoric and epistemic parts), are here 'converted' to weights in order to fit with the classification scheme and give a consistent result to combine with the other turbulence model. In this way we can classify uncertainty for the ensemble of turbulence models used in GASP, to ultimately provide e.g. maps of uncertainty classes over the entire planet.

The uncertainty index matrix for the 16 surface/flow classes (area categories) is shown in Figure 8. One can see that the uncertainty in wind speed and shear exponent (alpha) are lumped together, because of the identical dimensionless sensitivity to each that arises in the corresponding derivatives. The combined contribution also depends on the modelled inhomogeneity-induced (terrain) turbulence T, whose calculation is also shown in the table.

Although the stability information ($1/L$ statistics) from GWA3 was unable to be employed here due to inconsistencies in the GWA calculations, we (must) still include the stability component, because [1] a default (global mean) stability needed to be assumed, and [2] there is a height-dependent uncertainty which arises due to stability even if it is *not used as an input*, as shown in Kelly et al. (2019). The "turbulent transport" uncertainty in Fig. 8 refers to the turbulence

Uncertainty Index Matrix (contains values between 1 (green category, low uncertainty) and 3 (red, high uncertainty))						
	Uncertainty for certain area category associated with…					
Area ID	U + alpha	1/L	Turbulent transport	U-dependence in sigma u90	c_sigmau90	Wavelet tile-edge patching
1	1.0	1.5	1.0	2.0	1.5	2.0
2	2.0	1.5	1.5	2.5	2.5	2.0
3	3.0	2.0	2.0	3.0	3.0	2.0
4	1.5	1.5	1.5	1.5	1.5	2.0
5	2.5	2.0	2.0	2.0	2.0	2.0
6	3.0	2.0	2.5	3.0	3.0	2.0
7	1.0	2.0	1.5	2.0	1.5	2.0
8	2.0	2.0	1.5	2.0	2.0	2.0
9	3.0	2.0	2.0	2.5	2.5	2.0
10	1.0	2.0	1.5	2.0	1.5	2.0
11	2.0	2.0	2.0	3.0	2.5	2.0
12	3.0	1.5	2.5	2.5	2.5	2.0
13	1.0	2.5	1.0	1.0	1.5	2.0
14	1.5	2.0	1.0	2.0	2.0	2.0
15	1.5	2.0	1.0	2.0	2.0	2.0
16	2.0	2.0	1.5	3.0	2.5	2.0

Figure 8: Uncertainty index matrix for turbulence method-2, with 6 lumped contributions due to the various input and model parameters. Area ID's are the same as Fig. 3

model component addressing the effect of surface inhomogeneities and terrain complexity; U-dependence and $c_{\sigma_{U90}}$ refer to the coefficients in the linear model for $\sigma_{u,90\%}$ (which is convertible to/from σ_σ) and the wavelet tile-edge patching mostly affects α.

Matrix of un-normalized Weights (dynamic, based on sensitivity coeff's; must be normalized by sum at each point in order to add to 1)						
	Weight associated with a certain uncertainty category …					
Area ID	U + alpha	1/L	Turbulent transport	U-dependence in sigma u90	c_sigmau90	Wavelet tile-edge patching
1	dynamic:	dynamic:	dynamic:	dynamic:	1.00	0.00
2	1/[1+T/(U*alpha)]	1/(1+100/z)	T/(1+T)		1.00	0.00
3	where		where	Vref / U	1.00	0.00
4	T ~= 0.4*tanh(RIX/10%)		T defined		1.00	0.00
5	and where		in terms of	where	1.00	0.00
6	U is avg. speed		RIX at left	Vref is	1.00	0.00
7	alpha is avg.			turbine	1.00	0.00
8				operational	1.00	0.00
9				speed	1.00	0.00
10				(default:	1.00	0.00
11				12 m/s)	1.00	0.00
12					1.00	0.00
13					1.00	0.00
14					1.00	0.00
15					1.00	0.00
16					1.00	0.00

Figure 9: Weighting coefficients corresponding to the uncertainty contributions in Fig. 8. Area ID's are the same as previous figures

The dynamically determined weights are found for each evaluation point on the computational grid covering the planet. Note that the weights as shown in Figure 9 do not sum to 1; rather, they are normalized at each point. The scale of 100 m shown in the height-dependent stability uncertainty weighting arises from the standard deviation of global CFSR and WRF values, relative to the default effective inverse Obukhov length employed in this turbulence model for GASP. The tile-edge patching refers to the uncertainty to filtering, which has been included in the initial form of the uncertainty classification, but has been omitted at later stage. This is consistent with

Method-1 where effects due to the wavelet filtering have not been included.

2.4.3 Combined *UI* for Turbulence

After calculating the UI for turbulence with the two methods described in the previous section, the results are combined to a single representative value as follow: Over water (that is area IDs 13 to 16), the combined results UI_{comb} are the UIs from method 1, since method 2 has not been used over water. Over land (that is area IDs 1 to 12), the combined result UI_{comb} is constructed as the average of the UIs from method 1 and method 2.

2.5 Mapping of *UI* to three-class traffic light color scheme

As final step, the value range of the globally calculated UIs (by definition between 1 and 3) has been grouped into three discrete color categories to obtain the desired traffic light categorization (color classes green, orange and red). The definition / interpretation of each color class as well as the associated ranges of UI that are included in the color class are given in Table 3. Since the uncertainty classification of the 50-year wind and the combined turbulence has been performed independently, slightly different thresholds have been chosen to maintain the definition / interpretation of the three color classes for the particular siting parameter.

Table 3: Definition, description and ranges of UI associated with each of the three final uncertainty color classes

Categories	Interpretation	Associated UI range	
		V50	Turbulence
Green (color class 1)	Model chain and/or assumptions within range of applicability	[1, 1.6)	[1, 1.5)
Orange (color class 2)	Model chain and/or assumptions at the limit of applicability	[1.6, 2.5)	[1.5, 2.5)
Red (color class 2)	Model chain and/or assumptions likely outside range of applicability	[2.5, 3]	[2.5, 3]

3 Results

Figure 10 and Figure 11 show the final three-class uncertainty classification for the 50-year wind and the turbulence, respectively. Critical regions like the tropical-cyclone (TC) affected areas in the Pacific and Atlantic as well as highly complex terrain areas like the Andes or the Himalaya region are clearly identifiable. Similarly, near-shore areas (land and water) outside the TC-affected areas are identified as category 2 for the 50-year wind.

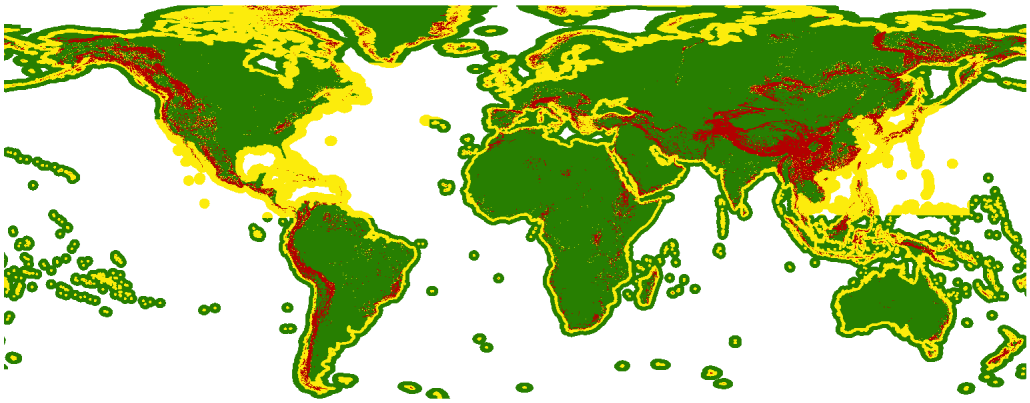

Figure 10: Depiction of the three uncertainty color classes for the 50-year wind (V50) over the globe. The definition of the colors follows the definition in Table 3.

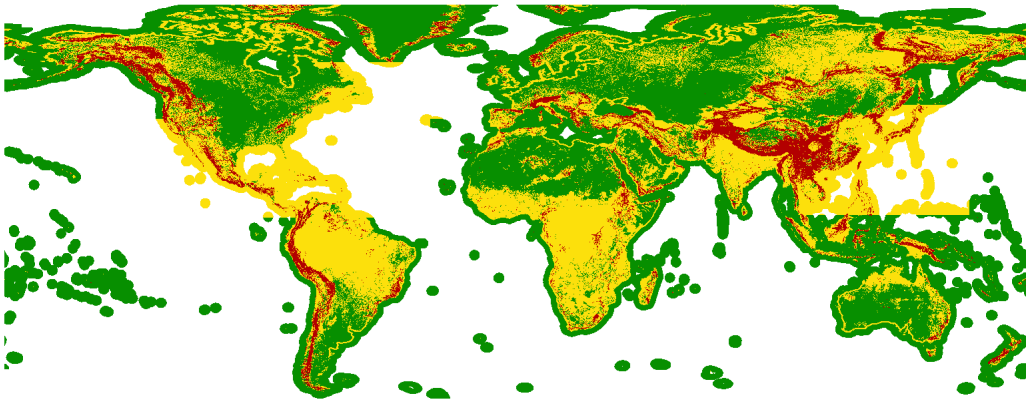

Figure 11: Depiction of the three uncertainty color classes for the turbulence over the globe. The definition of the colors follows the definition in Table 3.

The final three-class uncertainty classification layer over the globe shown in Fig. 10 and Fig. 11 are part of the GASP dataset (Larsén et al., 2021) and can be accessed via `https://doi.org/10.11583/DTU.14753349`

References

ESA (2017). Land Cover CCI Product User Guide Version 2. Technical report. Available at: maps.elie.ucl.ac.be/CCI/viewer/download/ESACCI-LC-Ph2-PUGv2_2.0.pdf.

Hill, C., DeLuca, C., Balaji, Suarez, M., and Da Silva, A. (2004). The architecture of the Earth system modeling framework. *Comput Sci Eng.*, 6(1):18–28.

JCGM (2008). Evaluation of measurement data — Guide to the expression of uncertainty in measurement (GUM). Technical Report JCGM 100:2008, Joint Committee for Guides in Metrology.

Kelly, M. (2020). Estimation of local turbulence intensity via mesoscale stability and winds, with microscale shear and terrain. Technical Report E-0213(EN), Wind Energy Dept., Risø Lab/Campus, Danish Tech. Univ. (DTU), Roskilde, Denmark.

Kelly, M., Kersting, G., Mazoyer, P., Yang, C., Fillols, F. H., Clark, S., and Matos, J. C. (2019). Uncertainty in vertical extrapolation of measured wind speed via shear. Technical Report E-0195(EN), Wind Energy Dept., Risø Lab/Campus, Danish Tech. Univ. (DTU), Roskilde, Denmark.

Larsén, X., Davis, N., Hannesdottir, A., Kelly, M., Olsen, B., Floors, R., Nielsen, M., and Imberger, M. (2021). Calculation of global atlas of siting parameters. Technical Report DTU Wind Energy E-0208, DTU Wind Energy Department.

Larsén, X. G., Davis, N., Hannesdóttir, Á., Kelly, M., Svenningsen, L., Meklenborg Miltersen Slot, R., Imberger, M., Olsen, B. T., Floors, R. R., Guldager Sørensen, T., and Thøgersen, M. (2021). Global atlas of siting parameters v1. URL https://doi.org/10.11583/DTU.14753349. DOI 10.11583/DTU.14753349.

Mortensen, N. G., Bowen, A. J., and Antoniou, I. (2006). Improving wasp predictions in (too) complex terrain. In *European Wind Energy Conference 2006*, Athens, Greece. European Wind Energy Association (EWEA).

Saha, S., Moorthi, S., Pan, H.-L., Wu, X., Wang, J., Nadiga, S., Tripp, P., Kistler, R., Woollen, J., Behringer, D., Liu, H., Stokes, D., Grumbine, R., Gayno, G., Wang, J., Hou, Y.-T., Chuang, H.-Y., Juang, H.-M. H., Sela, J., Iredell, M., Treadon, R., Kleist, D., Delst, P. V., Keyser, D., Derber, J., Ek, M., Meng, J., Wei, H., Yang, R., Lord, S., van den Dool, H., Kumar, A., Wang, W., Long, C., Chelliah, M., Xue, Y., Huang, B., Schemm, J.-K., Ebisuzaki, W., Lin, R., Xie, P., Chen, M., Zhou, S., Higgins, W., Zou, C.-Z., Liu, Q., Chen, Y., Han, Y., Cucurull, L., Reynolds, R. W., Rutledge, G., and Goldberg, M. (2010). NCEP climate forecast system reanalysis (CFSR) selected hourly time-series products, January 1979 to December 2010. URL https://doi.org/10.5065/D6513W89. DOI 10.5065/D6513W89.